

An improved nonlinear modelling and identification methodology of a servo-pneumatic actuating system with complex internal design for high-accuracy motion control applications

Ciprian-Radu Rad*, Olimpiu Hancu

Department of Mechatronics and Machine Dynamics, Faculty of Mechanical Engineering, Technical University of Cluj-Napoca, Romania



ARTICLE INFO

Article history:

Received 19 November 2016

Revised 22 February 2017

Accepted 20 March 2017

Available online 2 April 2017

Keywords:

Servo-pneumatics
Modelling
Identification
Simulation
Motion control

ABSTRACT

Precise and smooth motion control of servo-pneumatic actuating systems can be improved only by using appropriate mathematical models and identification procedures. In this paper, an improved modelling and parameter identification methodology of a servo-pneumatic linear drive unit with complex internal design that takes into account the influence of dead volume in terms of system dynamics has been developed. The proposed modelling methodology considers the nonlinear mass flow characteristic, dead zone of the valve, polytropic temperature model, heat transfer and nonlinear friction behavior. Experimental results indicates that a proper identification of the dead volume improves model accuracy in terms of pressure dynamics, piston velocity and piston position and therefore the proposed modelling methodology can be a good starting point to design better motion controllers in the field of servo-pneumatic actuating systems.

© 2017 The Authors. Published by Elsevier B.V.
This is an open access article under the CC BY-NC-ND license

(<http://creativecommons.org/licenses/by-nc-nd/4.0/>)

1. Introduction

Nowadays, approximatively 70% of servo control applications from industry move loads with a mass between 1–10 kg and with a level of precision between ± 0.02 and ± 0.2 mm [1]. Pneumatic actuators can be an important choice for this type of applications due to their simplicity, low sensitivity to high temperature variations, low-cost price/maintenance, power density and high travel speeds (up to 5 m/s). Moreover, they have the unique property of being irreplaceable in applications with radioactive and explosive risks or where strict conditions regarding shocks or vibrations are required [2].

However, pneumatic actuators exhibit highly nonlinear behavior given by: air compressibility, friction force, dead zone of proportional valve and mass flow rate characteristic; these being the main reasons why they are used mainly in pick and place applications and not in motion control ones. Precise and smooth motion control of servo-pneumatic actuating systems can be improved only by using appropriate mathematical models and experimental identification procedures [3–5]. A detailed analysis of servo-pneumatics modeling techniques is presented in [6,7]. The following conclusions can be drawn.

* Corresponding author.

E-mail address: ciprian.rad@mdm.utcluj.ro (C.-R. Rad).

Nomenclature

Symbol	Description	Unit
$i = a, b$	subscript for pneumatic chambers	
j, k	subscripts for proportional valve connection ports	
$\dot{m}_{i_{in}}, \dot{m}_{i_{out}}$	inlet and outlet mass flow rate Kg/s	
u	proportional valve input signal V	
$A_{j-k}(u)$	flow area as a function of signal u m ²	
C_d	discharge coefficient	
γ	ratio of specific heats	
P_s	supply pressure Pa	
T_s	supply temperature K	
P_i	chamber i pressure Pa	
T_i	chamber i temperature K	
P_0	equilibrium pressure Pa	
T_0	equilibrium temperature K	
V_i	chamber i volume m ³	
V_c	chamber under test volume m ³	
V_{id}	chamber i dead volume m ³	
V_p	volume generated by piston stroke m ³	
S_p	piston effective area m ²	
d_p	piston diameter m	
L_p	piston stroke m	
y	piston position m	
\dot{Q}_i	heat transfer between air from chamber i and cylinder wall J/s	
n	polytropic index	
λ_0	heat transfer coefficient at equilibrium pressure and temperature W/m ² .K	
$A_{q_i}(y)$	heat transfer area as a function of piston position m ²	
λ_{0r}	FESTO CRVZS-0.4 heat transfer coefficient W/m ² .K	
A_{q_r}	FESTO CRVZS-0.4 heat transfer area m ²	
P_{atm}	atmospheric pressure Pa	
ψ	mass flow rate function	
$b_{j-k}(u)$	critical pressure ratio as a function of input signal	
$a_{j-k}(u)$	cracking pressure ratio as a function of input signal	
$ms_{j-k}(u)$	subsonic index as a function of input signal	
β_{lam}	critical pressure ratio for laminar flow	
M_p	piston mass Kg	
\dot{y}	piston velocity m/s	
F_p	pneumatic force N	
F_e	external force N	
F_f	friction force N	
σ_0	stiffness coefficient of friction force N/m	
σ_1	damping coefficient of friction force N/m	
σ_2	viscous coefficient of friction force N·s/m	
F_s	level of stiction force N	
F_c	Coulomb friction force N	
\dot{y}_s	Striebeck velocity m/s	
z	internal state of friction force	
z_{ba}	stiction coefficient -	
zms	dead zone left limit V	
zmd	dead zone right limit V	
ms	dead zone left slope	
md	dead zone right slope	
u_0	pneumatic null V	
R	gas constant J/Kg·K	
A_{max}	maximum area of proportional valve ports m ²	
d_o	diameter of the proportional valve ports m	
C	sonic conductance of the proportional valve l/bar·s	
ρ_{ISO}	ISO 6358 density Kg/m ³	

T_{ISO}	ISO 6358 temperature K
<i>Constants</i>	
γ	1.4
n	1.35 [3]
R	288 J/Kg.K
P_s	7×10^5 Pa (absolute)
T_s	293.15 K
P_{atm}	1×10^5 Pa
L_p	290×10^{-3} m
d_p	25×10^{-3} m
S_p	4.9087×10^{-4} m ²
M_p	2.22 kg
$V_p = S_p \cdot L_p = \frac{\pi \cdot d_p^2}{4} L_p$	1.4235×10^{-4} m ³
C	3.1 l/bar.s [26]
d_o	6×10^{-3} m
$A_{max} = \frac{\pi \cdot d_o^2}{4}$	2.8274×10^{-5} m ²
ρ_{ISO}	1.185 Kg/m ³
T_{ISO}	293.15 K
P_{cr}	0.528
$C_1 = \sqrt{\frac{\gamma}{R} \left(\frac{2}{\gamma+1} \right)^{\frac{\gamma+1}{\gamma-1}}}$	0.0404
$C_d = \frac{C \cdot \rho_{ISO} \sqrt{T_{ISO}}}{A_{max} \cdot C_1}$	0.5513 [10]
$\lambda_{0,r}$	17.275 W/ m ² .K
$A_{q,r}$	3.419×10^{-2} m ²
P_0	5.65×10^5 Pa (absolute)
T_0	293.15 K
zba	$0.9 \cdot z_{max}$ [24]
$V_{CRVZS-04}$	0.344 m ³

Although Rao and Bone [8] states that mass flow characteristic is the key element of the mathematical model, standard orifice flow model is widely used in literature despite of its inability to take into account the reduction of critical pressure ratio for example [9,10]. Other papers use ISO 6358–1989 model which takes into account two parameters to describe the flow characteristic of pneumatic components: sonic conductance C and critical pressure ratio b . However, modern servo-pneumatic actuating systems include also silencers, multiple fittings and different tubing lengths which increase the flow resistance. This type of circuits are better represented by a cascade of orifices, nozzles or both as it is emphasized in [9,10]. The revised standard ISO 6358–1:2013 [11] adds two more parameters: cracking pressure ratio a and subsonic flow index ms . Cracking pressure ratio a is important because proportional valves have air leakages that determine an equilibrium pressure when the spool is at the central position (mass flow rate becomes zero for a pressure ratio less than one), while subsonic flow index ms is needed to accurately model the subsonic flow region when multiple restrictions are within the flow path. Therefore, the model used in this paper will take into account also the two additional parameters.

In addition, most thermodynamics models are simplified by neglecting heat transfer and assume isothermal or adiabatic process. This is due to the fact that heat transfer coefficient can be difficult to be measured because varies with pressure, temperature and speed of the piston. However, the polytropic model proposed by Carneiro and de Almeida in [12] has shown that by using a variable heat transfer coefficient that varies with pressure and temperature, the predication of pressure inside the actuator chambers is improved significantly. Moreover, the accuracy of the polytropic model can be further improved by considering the dead volume of pneumatic chambers [9].

Dead volume, i.e. the gas volume when the piston has contact with the end cover can vary significantly from one actuator to another and even if the dimensions of the cylinder are identical there remain a lot of differences between manufacturers especially if the internal design is highly complex [13]. In the context of high-accuracy motion control applications dead volume is very important because: (1) influence the dynamic response of the cylinder and consequently the accuracy of piston velocity and position (2) the stiffness of the cylinder changes along the stroke and dead volumes at the end positions play a relatively important role [14] and (3) otherwise an effective volume of zero would occur during simulations when the piston has reached an end position [13]. The major problem is that manufacturers does not provide this parameter and although in the case of pneumatic actuators with a complex internal design this parameter cannot be easily computed [13], we noticed that in many papers [3,16] is given without any explanations of how was determined. Therefore in this paper we will use the original experimental procedure reported in our previous work [17] to easily and accurately determine the dead volume in a pneumatic linear drive unit with complex internal design and show its influence on system dynamics.

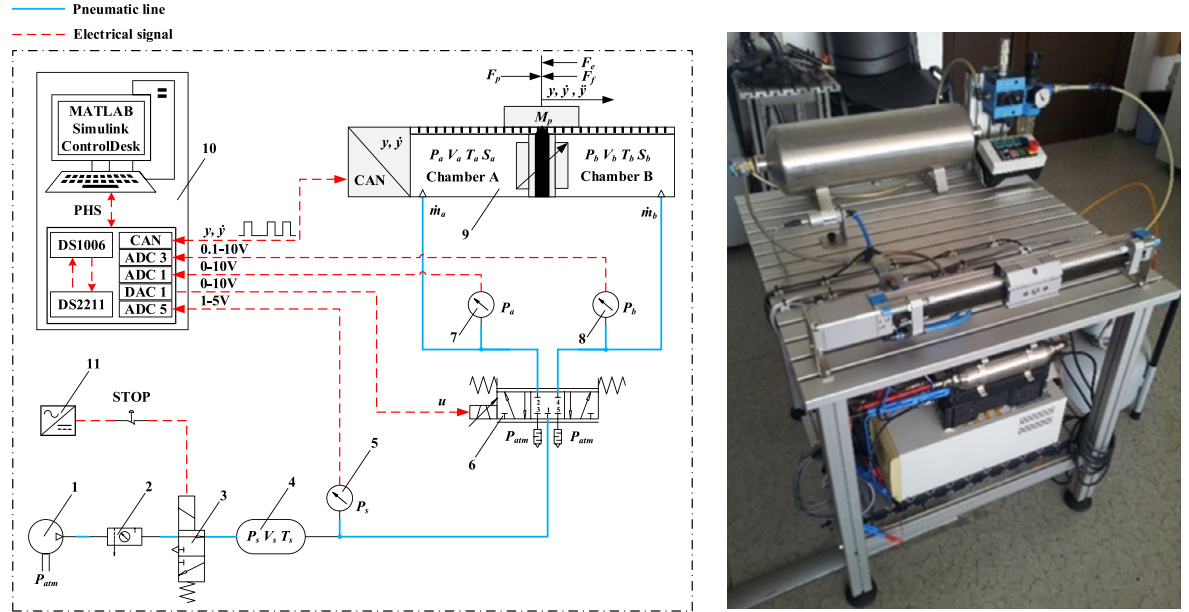


Fig. 1. Experimental set-up.

The experimental procedure is very useful in the case of pneumatic actuators with very complex internal design but can be equally applied on simpler pneumatic actuators too.

Finally, it is generally accepted that friction force is the main nonlinearity in linear pneumatic actuators and generates positioning errors, tracking errors, oscillations near equilibrium point and stick slip motion [4,18,19]. It is also known that friction force is a function of velocity, load, displacement, temperature of two contact surfaces, and the surface properties, many of which are time dependent and/or temperature dependent [20]. Therefore, accurate modeling of friction is not an easy task. In this context, it is very important to fully understand it in order to compensate it and design better motion control systems. Many researchers have addressed the problem of friction in pneumatic actuators by using classical friction models [4,6–9], although these models are suitable mainly for low friction pneumatic actuators. On the other side, dynamic models such as Dahl model, LuGre model, Elastoplastic friction model, Leuven model or Generalized Maxwell-Slip model offers better results in the case of highly precision actuators [3,20,24]. Therefore, the dynamic Elastoplastic friction model will be used in this paper due to the fact that: (1) has the advantage of overcoming the drift problem of Dahl and LuGre models by defining a stiction zone [21–23] and (2) more recently Richter et al. [24] used it with success to model friction force in special pneumatic actuators.

To conclude, the purpose of this study is to provide an improved modelling and parameter identification methodology of a servo-pneumatic linear drive unit with complex internal design. Methodology takes into consideration also the influence of dead volume in terms of system dynamics and includes the latest 5 years contributions in the area of servo-pneumatics. Experimental results were compared with results obtained by numerical simulation and the analysis indicates that a proper identification of the dead volume improves model accuracy in terms of pressure dynamics, piston velocity and piston position. Therefore the proposed modelling methodology can be a good starting point to design better motion controllers in the field of servo-pneumatic actuating systems.

The rest of the paper is structured as follows: in [Section 2](#) the experimental setup is presented. Mathematical model is derived in [Section 3](#) while parameter identification is detailed in [Section 4](#). The influence of dead volume on system dynamics is evaluated in [Section 5](#) and experimental results are presented in [Section 6](#). Finally, the paper end up with the conclusions.

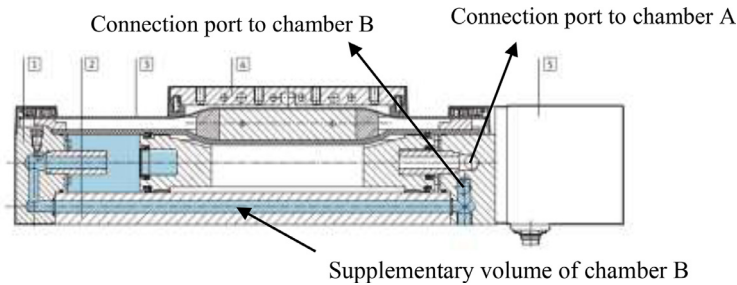
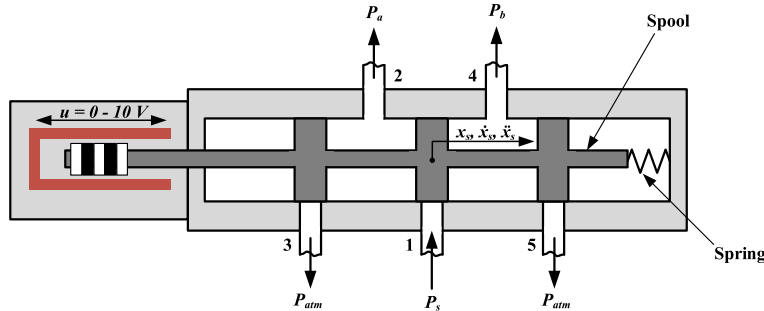
2. Experimental set-up

[Fig. 1](#) presents the schematic representation of experimental set-up while [Table 1](#) presents the main components. The servo-pneumatic actuating system consists of a rodless pneumatic linear drive unit 9 controlled by a five-way proportional directional control valve 6. Air supply is generated by compressor 1 and filtered by air service unit 2. The pneumatic pipes were kept as short as possible in order to minimize the effects of delays and losses described by Richer and Hurmuzulu in [15]. A buffer reservoir 4 has been introduced in the pneumatic circuit in order to minimize pressure supply variation. Pressure supply and the pressure from both chambers are measured with pressure sensors 5, 7 and 8 respectively. Position and velocity of the piston is measured with an integrated MTS sensor based on temposonics technology with a precision of 5 μm . Signals of pressure sensors and input signal of proportional directional control valve are analogue, while position and

Table 1

The main components of the experimental set-up.

No.	Component	Model
1	Compressor	JUN-AIR Model 6-25
2	Air service unit	FESTO LFR-d-3/8-S-B
3	3/2 safety valve	FESTO MFHE-3-3/8
4	Buffer reservoir	FESTO CRVZS-10
5	Pressure sensor	FESTO SDE-10-5 V/20mA
6	Proportional directional control valve	FESTO MPYE-5-1/8-HF-010-B
7	Pressure sensor	FESTO SDE-10-10 V/20 mA
8	Pressure sensor	FESTO SDET-22T-D10-G14-U-M12
9	Rodless pneumatic linear drive unit	FESTO DGPIL-25-360-AIF-KF-AV
10	dSPACE modular system	dSPACE (DS1006, DS2211 and PC)
11	Power supply for emergency stop	FESTO TN 162,416
12	Power supply for proportional valve (not showing)	FESTO TN 162,416
13	Power supply for sensors (not showing)	FESTO TN 162,416

**Fig. 2.** Section view through the rodless pneumatic linear drive unit.**Fig. 3.** Conceptual representation of the proportional directional control valve.

velocity of the piston is transmitted digitally through a CAN bus. A dSPACE modular system 10 is used for DAQ. For safety reason, valve 3 can interrupt the pneumatic circuit when the user pushes the STOP button.

Fig. 2 presents a section view through the rodless pneumatic linear drive unit [25]. From the figure it is clear that internal design is very complex. Moreover, both connection ports are on the right side which generates an additional volume for chamber B.

3. Modelling methodology

The development of modelling methodology requires the following considerations: (1) the investigation of valve dynamics, (2) the determination of mass flow rate characteristic, (3) the thermodynamic model of the pneumatic chambers, (4) piston-load dynamics and (5) friction force model. The five combined models describe the entire mathematical model of the system.

3.1. Valve dynamics

Fig. 3 presents the conceptual representation of the proportional directional control valve. Mechanical part is responsible for the movement of the spool which is proportional with the input signal u , while pneumatic part describes the air flow through the four variable pneumatic resistances (**Fig. 4**) as a function of spool position. Valve dynamics was studied by Meng et al. in [3]. They concluded that static spool displacement characteristic is linear and has low hysteresis while critical

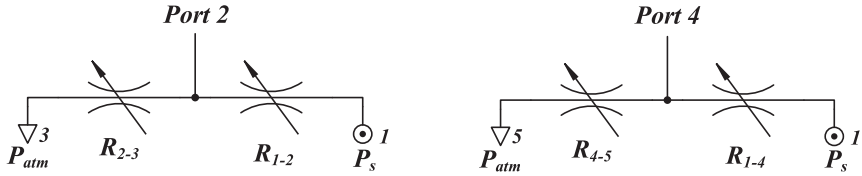


Fig. 4. The two half bridges of the proportional directional control valve.

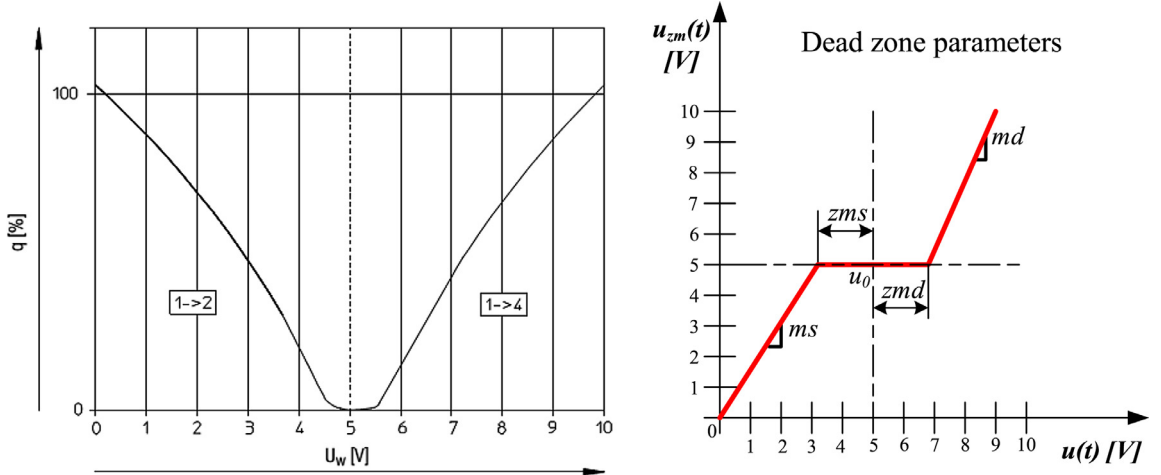


Fig. 5. Mass flow characteristic of the proportional directional control valve.

frequency is near 100 Hz. Since the bandwidth of a servo-pneumatic system is no more than 10 Hz and the critical frequency of the spool is 10 times greater, it is well known that dynamics of the spool can be neglected without introducing significant errors into the model [3,8].

3.2. Mass flow characteristics

Mass flow characteristic is the key element of the model. Fig. 5 presents the characteristic of the valve provided by manufacturer in datasheet [26]. From the figure it is clear that it depends on the spool position in a nonlinear way. Also the valve is a closed center one, has dead zone and pneumatic null is shifted. However, experimental set-up includes not only the proportional directional control valve but also silencers, multiple fittings and different tubing lengths which increases flow resistance. In this context, mass flow characteristic is modelled as a combination between standard orifice theory model and ISO 6358–1:2013. The proposed model has the advantage that can be used to predict the combined effect of the multiple restrictions within the flow path, the result being a single model that integrates the behavior of all restrictions as a merged orifice. The model consists of Eqs. (1), (2) and (3) and the influence of additional ISO 6358–1:2013 parameters is illustrated in Fig. 6. Due to the presence of silencers, fittings, different tubing lengths, etc. within the flow path, the main parameters of the model (A , b , a , ms) of every pneumatic resistance (R_{1-2} , R_{2-3} , R_{1-4} , R_{4-5}) will have to be identified both for charging and discharging.

$$\dot{m}_{i_{in}} = A_{j-k}(u) \cdot C_d \cdot C_1 \frac{P_s}{\sqrt{T_s}} \psi \left(\frac{P_{atm}}{P_i}, \frac{P_i}{P_s} \right) \quad (1)$$

$$\dot{m}_{i_{out}} = A_{j-k}(u) \cdot C_d \cdot C_1 \frac{P_i}{\sqrt{T_i}} \psi \left(\frac{P_{atm}}{P_i}, \frac{P_{atm}}{P_s} \right) \quad (2)$$

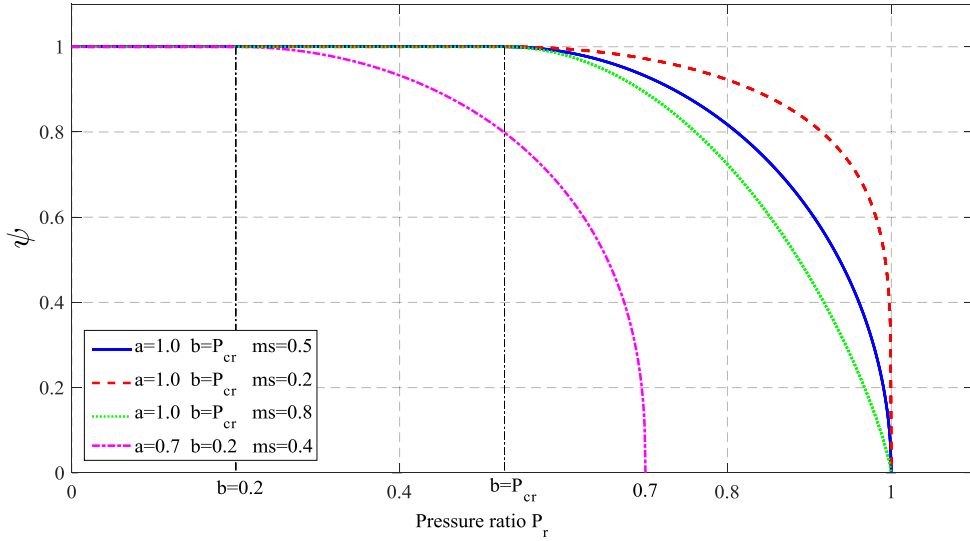


Fig. 6. The influence of ISO 6358-1:2013 parameters.

$$\psi(P_{min}, P_r) = \begin{cases} 1 & P_{min} \leq P_r \leq b_{j-k}(u) \\ \left[1 - \left(\frac{P_r - b_{j-k}(u)}{a_{j-k}(u) - b_{j-k}(u)} \right)^2 \right]^{ms_{j-k}(u)} & b_{j-k}(u) < P_r < \beta_{lam} \\ \left(\frac{1 - P_r}{1 - \beta_{lam}} \right) \left[1 - \left(\frac{\beta_{lam} - b_{j-k}(u)}{a_{j-k}(u) - b_{j-k}(u)} \right)^2 \right]^{ms_{j-k}(u)} & \beta_{lam} \leq P_r \leq 1 \end{cases} \quad (3)$$

R_{j-k}	i	j	k
1-2	a	1	2
2-3	a	2	3
1-4	b	1	4
4-5	b	4	5

3.3. Thermodynamic model of the pneumatic chambers

It is generally accepted that the behavior of the compressed air inside the pneumatic chambers of a cylinder it is fully described by the following set of Equations [12]:

$$\begin{cases} \dot{P}_i = -\gamma \frac{P_i}{V_i} \dot{V}_i + \dot{m}_{i_{in}} \frac{R \cdot T_s}{V_i} \gamma - \dot{m}_{i_{out}} \frac{R \cdot T_i}{V_i} \gamma + \frac{\gamma - 1}{V_i} \dot{Q}_i \\ \dot{T}_i = \frac{T_i}{V_i} \dot{V}_i (1 - \gamma) + \dot{m}_{i_{in}} \frac{R \cdot T_i}{P_i \cdot V_i} (\gamma \cdot T_s - T_i) - \dot{m}_{i_{out}} \frac{R \cdot T_i^2}{P_i \cdot V_i} (\gamma - 1) + \frac{(\gamma - 1) T_i}{P_i \cdot V_i} \dot{Q}_i \end{cases} \quad (4)$$

where:

$$\begin{cases} V_a = V_{ad} + S_p \cdot y \\ V_b = V_{bd} + S_p (L_p - y) \end{cases} \quad (5)$$

$$\dot{Q}_i = \lambda_0 \cdot A_{q_i}(y) \cdot \sqrt{\frac{P_i \cdot T_i}{P_0 \cdot T_0}} \cdot (T_s - T_i) \quad (6)$$

$$\begin{cases} A_{q_a}(y) = 2 \cdot S_p + \pi \cdot d_p \cdot y \\ A_{q_b}(y) = 2 \cdot S_p + \pi \cdot d_p (L_p - y) \end{cases} \quad (7)$$

However, model described by Eq. (4) is too complex to be used for controller design since the heat transfer coefficient is very difficult to measure due to the fact that varies with temperature, pressure and piston velocity. Recent research conducted by Carneiro has shown that by using a polytropic temperature process with a tunable index n and a simplified Eichelberg heat transfer model that neglects the temperature and pressure variations with respect to their equilibrium values, best results in terms of model performance/complexity is achieved [12]. The polytropic model is described by Eq. 8 and the main problem is to determine the heat transfer coefficient λ_0 at equilibrium point (P_0, T_0) . Moreover, chambers total

volume is influenced by dead volumes so if the parameter is correctly identified the accuracy of the polytropic model can be improved.

$$\begin{cases} T_i = T_s \left(\frac{P_i}{P_0} \right)^{(n-1)/n} \\ \dot{P}_i = -\gamma \frac{P_i}{V_i} \dot{V}_i + \dot{m}_{i_{in}} \frac{R \cdot T_s}{V_i} \gamma - \dot{m}_{i_{out}} \frac{R \cdot T_i}{V_i} \gamma + \frac{\gamma - 1}{V_i} A_{q_i}(y) \cdot \lambda_0 \sqrt{\frac{P_i \cdot T_i}{P_0 \cdot T_0}} \cdot (T_s - T_i) \end{cases} \quad (8)$$

3.3. Piston dynamics and friction force model

Piston motion can be described using Newton's second law:

$$M_p \cdot \ddot{y} = F_p - F_e - F_f = S_p(P_a - P_b) - F_e - F_f \quad (9)$$

The first term from the right side represents the pneumatic force generated by the pressure difference from both chambers, second one take into account the external forces but due to the fact that actuator is orientated horizontally the external force is zero, while the last term is friction force. Friction force is modelled using Elasto-plastic friction model (Eq. 10):

$$\begin{cases} F_f = \sigma_0 \cdot z + \sigma_1 \frac{dz}{dt} + \sigma_2 \cdot \dot{y} \\ \frac{dz}{dt} = \dot{y} - \alpha(z, \dot{y}) \frac{\sigma_0}{g_{ss}(\dot{y})} |\dot{y}| \cdot z \end{cases} \quad (10)$$

Where the term $\alpha(z, \dot{y})$ is a continuous function proposed by Dupont [21–23] to describe stiction.

$$\alpha(z, \dot{y}) = \begin{cases} 0, & |z| \leq z_{ba} \\ 0 < \frac{1}{2} \sin \left(\pi \frac{|z| - \left(\frac{z_{max}(\dot{y}) + z_{ba}}{2} \right)}{z_{max}(\dot{y}) - z_{ba}} \right) + \frac{1}{2} < 1, & z_{ba} < |z| < z_{max}(\dot{y}) \\ 1, & |z| \geq z_{max}(\dot{y}) \\ 0, & sign(\dot{y}) \neq sign(z) \end{cases} \quad (11)$$

$$0 < z_{ba} < z_{max}(\dot{y}) = \left| \frac{g_{ss}(\dot{y})}{\sigma_0} \right| \text{ for } \forall \dot{y} \in \mathfrak{N}$$

The term $g_{ss}(\dot{y})$ describes the steady state part of the friction model and uses static Stribeck curve:

$$g_{ss}(\dot{y}) = F_c + (F_s - F_c) e^{-\left(\frac{\dot{y}}{y_s}\right)^2} \quad (12)$$

In steady state motion ($\dot{y} = const.$, $\alpha(z, \dot{y}) = 1$, $\dot{z} = 0$) internal state z can be written as follows:

$$z_{ss} = \frac{\dot{y}}{|\dot{y}|} \frac{g_{ss}(\dot{y})}{\sigma_0} = sign(\dot{y}) \frac{\left(F_c + (F_s - F_c) e^{-\left(\frac{\dot{y}}{y_s}\right)^2} \right)}{\sigma_0} \quad (13)$$

Finally, the relationship between friction force and piston velocity for steady state motion is given by the following equation:

$$F_{f_{ss}} = \sigma_0 \cdot z_{ss} + \sigma_1 \cdot 0 + \sigma_2 \cdot \dot{y} = sign(\dot{y}) \left(F_c + (F_s - F_c) e^{-\left(\frac{\dot{y}}{y_s}\right)^2} \right) + \sigma_2 \cdot \dot{y} \quad (14)$$

The dynamic elastoplastic friction model describes friction as a function of velocity, load and displacement and is able to represent its behavior very precisely. However, if highly accurate control is required the model can be further expanded by considering the influence of temperature on friction parameters. Li et al. studied in [20] the influence of temperature on LuGre friction model but their method can be extended to elastoplastic friction model as well. They concluded that best results in term of model performance/complexity is achieved by using a thermal model where friction parameters are temperature independent while a temperature-dependent function is added to the temperature-independent friction model. Eq. 15 presents the temperature dependent friction force model F_f^T where F_f^{EPF} is the friction force based on the temperature independent elastoplastic model described by Eq. 10 and ΔF_f^{TIF} is the so called thermal-induced friction force [20] which must be determined experimentally.

$$F_f^T = F_f^{EPF} + \Delta F_f^{TIF} \quad (15)$$

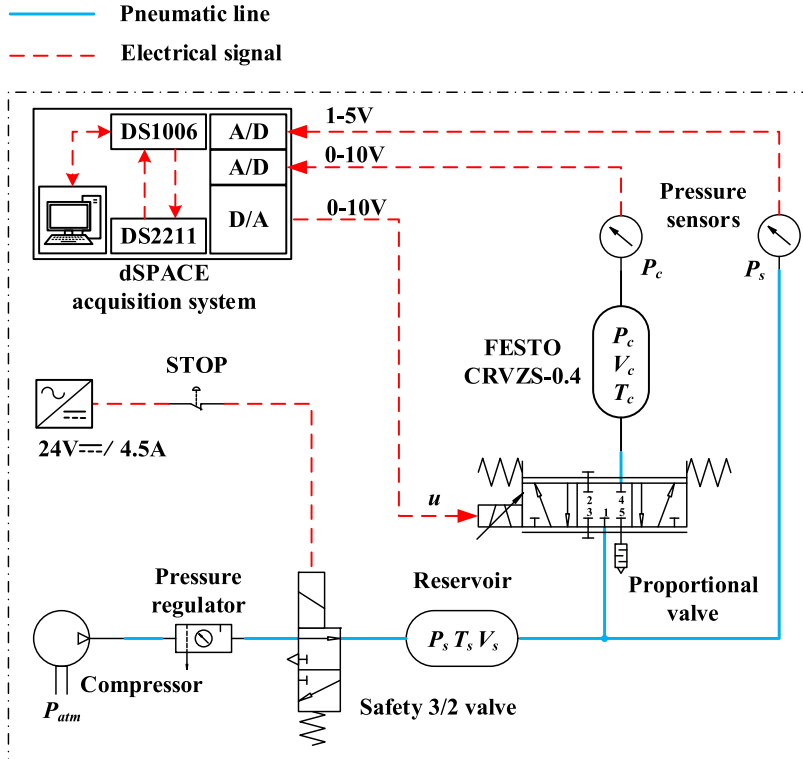
4. Parameter identification

In order to validate the model the main parameters of the experimental set-up must be known. Therefore, some parameters were obtained from components datasheets and mathematical relationships (see Nomenclature) and the unknown parameters (Table 2) were identified using experimental procedures described in this section.

Table 2

The unknown parameters of the model.

Proportional valve parameters	Pneumatic actuator parameters
zms, zmd, u_0, ms, md $R_{j-k}[A_{j-k}(u), b_{j-k}(u), a_{j-k}(u), ms_{j-k}(u)]$	V_a, V_b, V_{ad}, V_{bd} $\lambda_0 = \lambda(P_0, T_0)$ $\sigma_0, \sigma_1, \sigma_2, F_c, F_s, \dot{y}_s, \Delta F_j^{TIF}$

**Fig. 7.** Pneumatic circuit used for the identification of mass flow characteristic parameters.

4.1. Proportional valve parameters

Flow parameters of each pneumatic resistance are determined using an input/output gray-box identification procedure implemented in MATLAB/Simulink. The procedure is fully described in our previous works [29]. The procedure correspond to an inverse problem for determining the mass flow rate from the experimental transient pressure response within a constant volume reservoir connected to the investigated output port of the valve (Fig. 7) [24,25,27,28,30]. Both output ports were investigated separately for charging and discharging phases due to the silencers and multiple fittings on exhaust paths which increase the pneumatic resistance. The transient pressure curves are obtained experimentally by charging and discharging the reservoir connected to the output port. In the case of port 4 the following procedure was used. The pressure supply was set to 7 bar (absolute) and connecting tubes were kept as short as possible. A control signal between 5–10 V connects output port 4 to supply pressure (1→4) and between 0–5 V to atmosphere (4→5). The upstream pressure was considered pressure supply P_s for charging and pressure P_c for discharging. For discharging, the reservoir was initially fully filed in with a signal of 10 V and then the air was released into atmosphere. The tests were conducted over the entire range of input signal u with a step size of 0.2 V, resulting therefore 50 pressure curves P_c (Fig. 8) and 50 pressure curves P_s for output port 4. During the measurements, the unused ports were blocked. Port 2 was tested in same manner. Next, the mathematical model of the pneumatic circuit from Fig. 7 is implemented in MATLAB/Simulink based on equations from Section 3 and transient pressure curves P_s and P_c are used as input/output data for the model. Using Parameter Estimation tool from Simulink Design Optimization Toolbox, the flow parameters (A, b, a, ms) of each pneumatic resistance ($R_{1-2}, R_{2-3}, R_{1-4}, R_{4-5}$) are estimated simultaneously for each pair of input/output data using function lsqnonlin function. Fig. 9 presents two situation for charging and discharging output port 4 were the simulation response is compared with the experimental one after flow parameters identification. Effective area A is the most important parameter of the mass flow characteristic and it is presented in Fig. 10 as a function of input signal u for all pneumatic resistances. The obtained characteristic is very

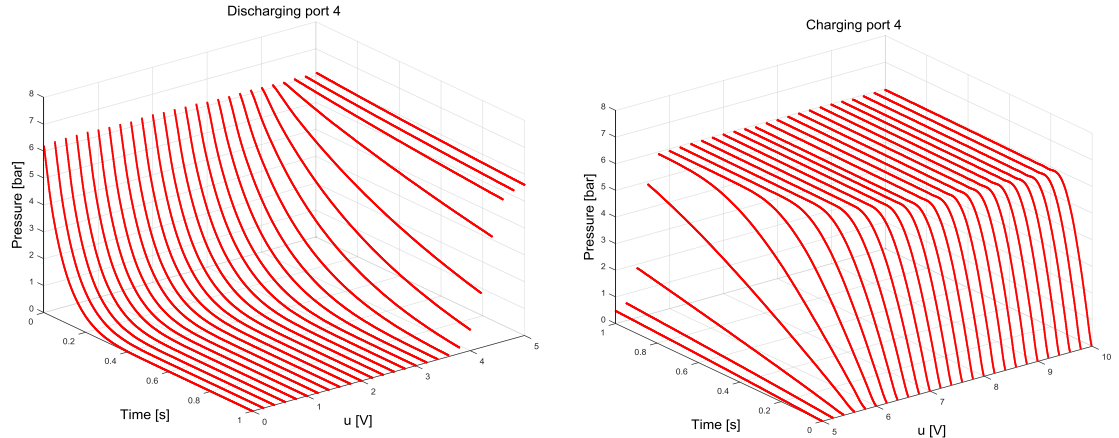


Fig. 8. Output port 4 – transient pressure curves obtained experimentally.

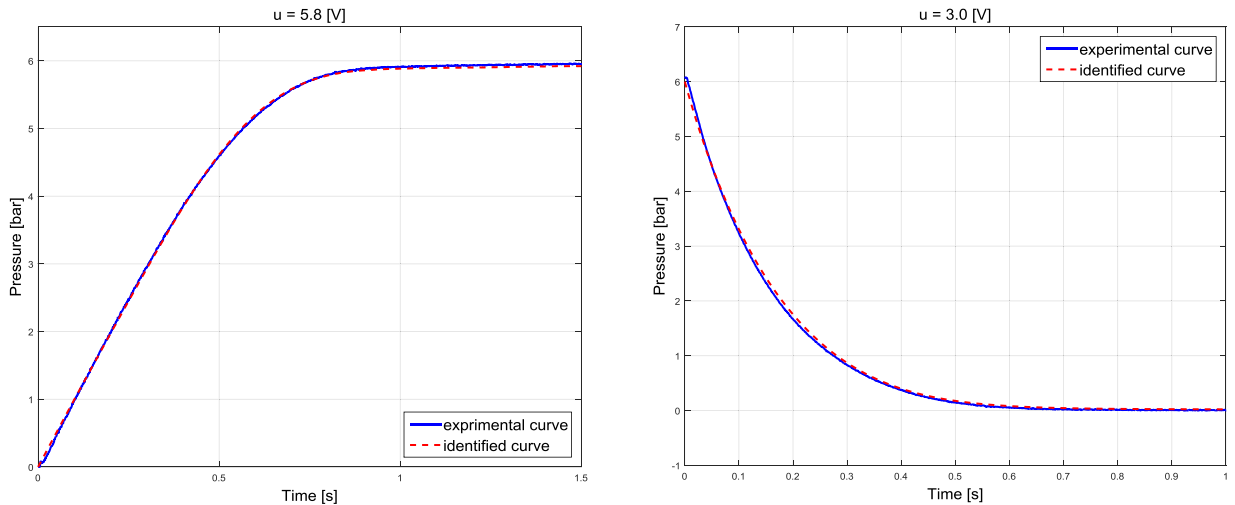


Fig. 9. Experimental vs simulated pressure curves.

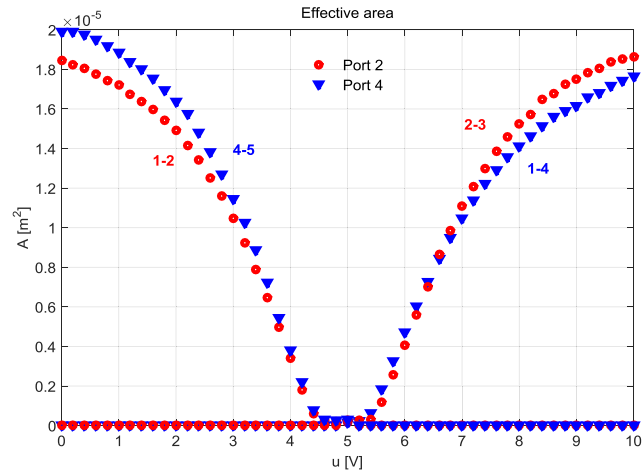


Fig. 10. Effective flow area $A(u)$ after identification.

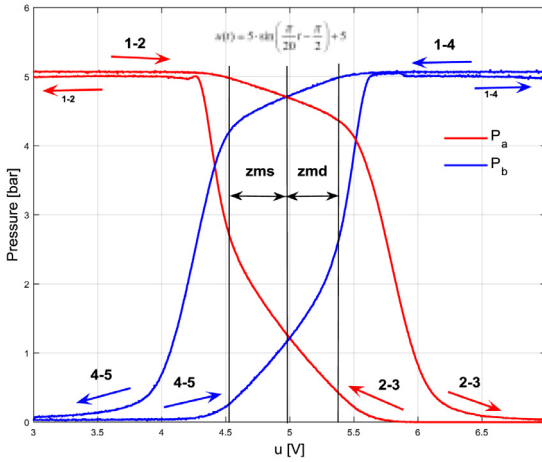


Fig. 11. Pressure vs input signal static map.

Table 3
Dead zone parameters.

Dead zone left limit zms [V]	4.53
Dead zone right limit zmd [V]	5.37
Dead zone left slope ms	1
Dead zone right slope md	1
Pneumatic null u_0 [V]	4.98

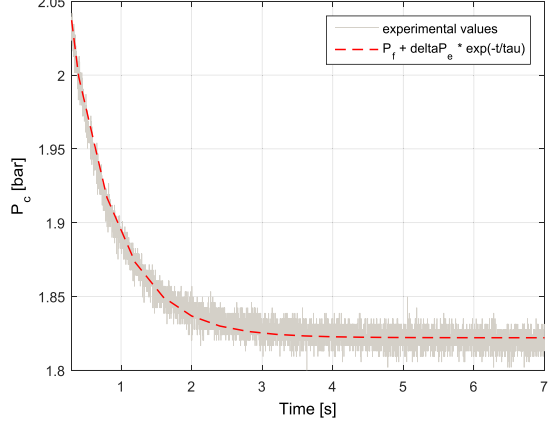
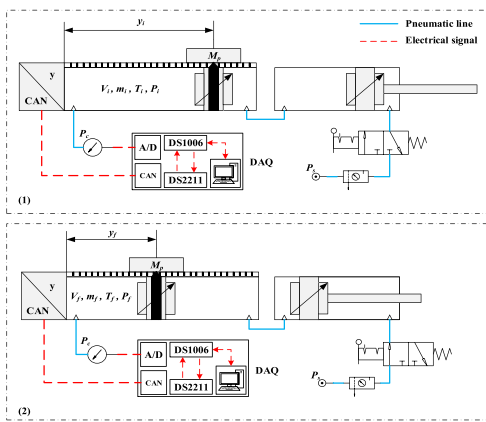


Fig. 12. Pneumatic circuit used to estimate thermal time constant.

similar with the one presented in Fig. 5. Its asymmetry is attributed to the different resistance on the exhaust paths mainly caused by the silencers and fittings. Rest of the parameters together with effective flow area were introduced then in lookup tables to be used for simulation purpose.

Finally, dead zone parameters illustrated in Fig. 5 are determined easily using the static map of chambers pressure vs. input signal u (Fig. 11) [31]. The characteristic can be easily obtained by applying a sinusoidal input signal on proportional valve and measure the pressure inside both chambers. Obtained results are presented in Table 3.

4.2. Linear drive unit parameters

In order to determine heat transfer coefficient between air from chamber and cylinder wall, thermal time constant τ of the pneumatic chamber must be known [32]. Thermal time constant is determined by fitting Eq. (16) to the pressure response of the air inside the chamber to a change in volume. Pneumatic circuit from Fig. 12 was used for this purpose. In phase (1), the piston of the linear drive unit was moved at position y_i and a pressure sensor was mounted on exhaust path and the other port was connected to another pneumatic cylinder. In phase (2), the piston was pushed by an external pneumatic force to the final position y_f . Pressure inside the chamber was measured until reached a stationary value and then

Table 4
Heat transfer characteristics.

Thermal time constant τ [s]	0.662
Average thermal conductance λ_{av} [W/K]	0.221
Average heat transfer coefficient λ_0 [W/K·m ²]	22.563

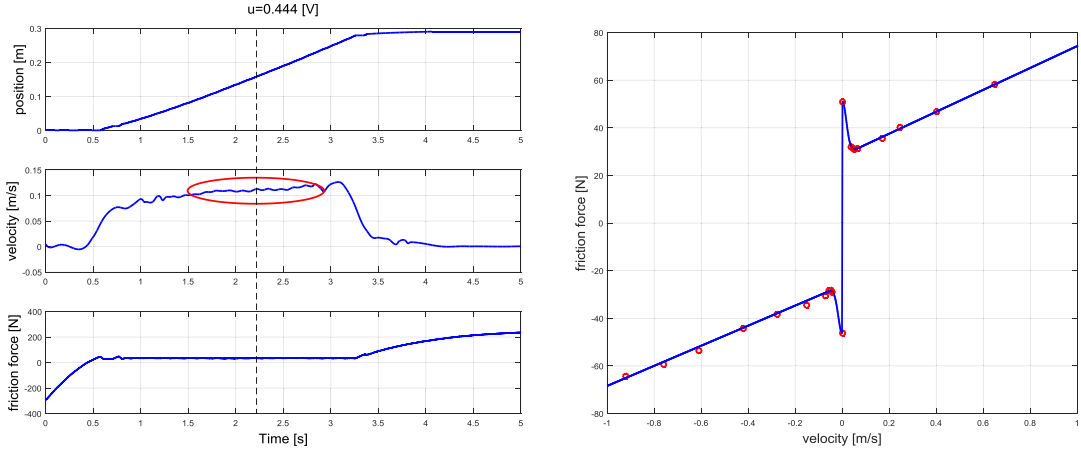


Fig. 13. Open loop tests to determine friction force vs. velocity static map.

was fitted to Eq. (16) in MATLAB using Curve Fitting Toolbox. Using thermal time constant, average thermal conductance k can be computed using Eq. (17) while average heat transfer coefficient λ_{av} is found with Eq. (18). Finally, average heat transfer coefficient λ_0 can be related with the equilibrium pressure and temperature conditions using Eq. (19). Final values are presented in Table 4.

$$\hat{P}(t) = \hat{P}_f + \Delta\hat{P}e^{-t/\tau} \quad (16)$$

$$\bar{k} = \frac{m \cdot c_v}{\tau} \quad (17)$$

$$\hat{\lambda}_{av} = \frac{\bar{k}}{A_q} \quad (18)$$

$$\hat{\lambda}_0 = \hat{\lambda}_{av} \sqrt{\frac{P_0 \cdot T_0}{\hat{P}_{av} \cdot \hat{T}_{av}}} \quad (19)$$

Next, static and dynamic parameters of friction force model are identified. Static parameters are estimated in steady-state piston motion when inertial term from Eq. (9) can be neglected (constant velocity), situation where friction force equals the resultant pneumatic force. To perform these type of tests a constant input signal u is applied on the proportional valve in such way that piston will travel most of its stroke with constant velocity (Fig. 13). For every input signal, pressure response from both chambers is measured and then friction force is calculated. Experimental points are then used then to obtain the static map of friction force vs. piston velocity (Fig. 13). The level of static friction force was determined from stick-slip motion. The input signal u applied on the proportional valve was chosen in that way to obtain the stick-slip motion as can be seen in Fig. 14. Note that static friction force is not constant and depends both on position and direction. Finally, Coulomb friction and Stribeck velocity are identified using Curve Fitting Toolbox from MATLAB. According to Valdiero [33], dynamic parameters can be related to static parameters. Stiffness coefficient can be adjusted using Eq. (20) based on the premise that the order of micro deformations z in the region of pre-sliding accept values in the range of 1 to 50 μm while damping coefficient is proportional to the pre-sliding displacement change rate and therefore can be obtained by Eq. (21). The final results are presented in Table 5.

Thermal-induced friction force ΔF_{TIF}^{TIF} can be determined from the static characteristic between displacement and temperature [20]. However, to evaluate experimentally this characteristic the entire system must be put in a temperature controlled chamber. The drawback of this procedure is evident in our particular situation and in this context thermal influence will not be included in the friction model. The improvement of the friction model, and the simulation and validation of temperature influence in the case of servo-pneumatic actuating systems will be subjects for future research.

$$\sigma_0 = \frac{F_c}{|1 \rightarrow 50| \cdot 10^{-6}} \quad (20)$$

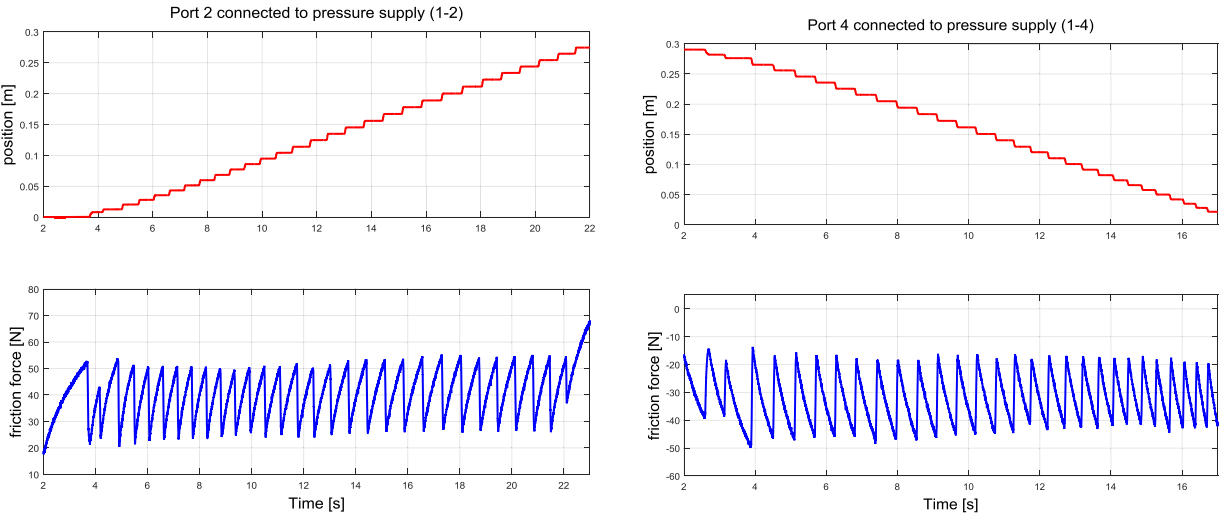


Fig. 14. Open loop test to determine static friction force level.

Table 5
Friction force parameters.

	$\dot{y} > 0$	$\dot{y} < 0$
Stiffness coefficient of friction force σ_0 [N/m]	$1.12 \cdot 10^6$	$-1.12 \cdot 10^6$
Damping coefficient of friction force σ_1 [N/m]	50	-50
Viscous coefficient of friction force σ_2 [N·s/m]	46.01	-42.18
Static friction force F_s [N]	50.97	-46.15
Coulomb friction force F_c [N]	28.35	-26.22
Stribeck velocity y_s [m/s]	0.024	-0.024

Table 6
Dead volumes and total volumes.

Total volume V_a [m^3]	$1.734 \cdot 10^{-4}$
Dead volume V_{ad} [m^3]	$3.125 \cdot 10^{-3}$
Total volume V_b [m^3]	$1.976 \cdot 10^{-4}$
Dead volume V_{bd} [m^3]	$5.530 \cdot 10^{-3}$

$$\sigma_1 \leq \frac{\sigma_2}{\left(\frac{F_s}{F_c} - 1\right)} \quad (21)$$

Finally, dead volumes must be identified. From author's knowledge, only Richer and Hurmuzulu in [15] have addressed the problem of dead volume identification in pneumatic actuators for simulation and control purposes. They suggested that if a detailed geometry of the actuator is available dead volumes can be computed easily, otherwise they can be computed by filling the ports cavities with a liquid (lubrication oil) and then measuring the volume of the used liquid. This method is difficult to apply and it is not a clean one. Therefore, the original experimental procedure reported in our previous work [17] will be used for this purpose.

The procedure is based on the assumption that if the piston chamber is considered a closed system, then the pressure exerted by a given mass of an ideal gas is inversely proportional to the volume it occupies (if the temperature and amount of gas remain unchanged). Fig. 15 presents the pneumatic circuit used to determine dead volume of chamber A for example. The piston was locked at one end and then connected to a filled air reservoir with known volume, pressure and temperature. If the air is released in the cylinder chamber and we wait enough time for the temperature to settle down and to be considered constant, total volume can be computed using pressure difference measured by the sensor (Eq. 22).

One important thing to note from the slope of the pressure curve in Fig. 13 is the presence of leakages which can affect volume measurements. However, between 20–30 s in this particular case, the pressure is approximately constant and so the value of P_2 was taken from that area. Dead volume is then calculated indirectly by subtracting the volume generated by the piston stroke from the chamber total volume (Eq. 23). We do this for two reasons: (1) since the dead volume is much smaller compared to the total volume, the pressure difference measured by the sensor would be also much smaller and together with the electrical noise from sensor can be an important source of errors and (2) the pneumatic chambers have leakages and small pressure difference influence the accuracy also in this case. Table 6 presents the final results. The

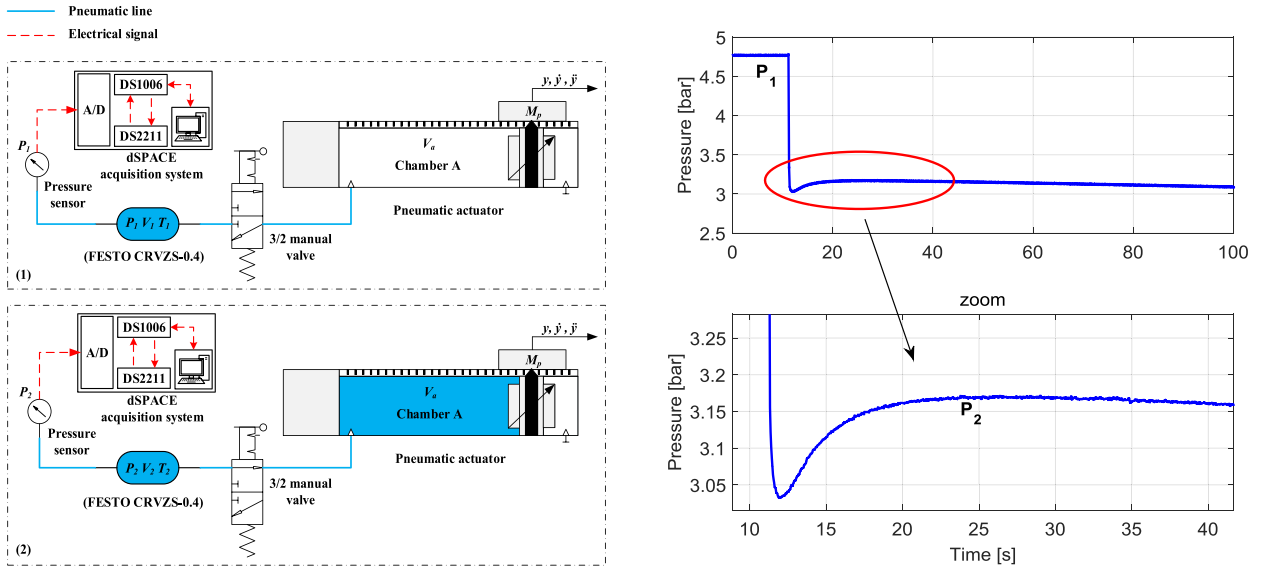


Fig. 15. Identification of dead volume V_{ad} .

obtained results confirm the situation from Fig. 2 where $V_{bd} > V_{ad}$.

$$V_i = V_2 - V_1 = V_1 \left(\frac{P_1}{P_2} - 1 \right) \quad (22)$$

$$V_{id} = V_i - V_p \quad (23)$$

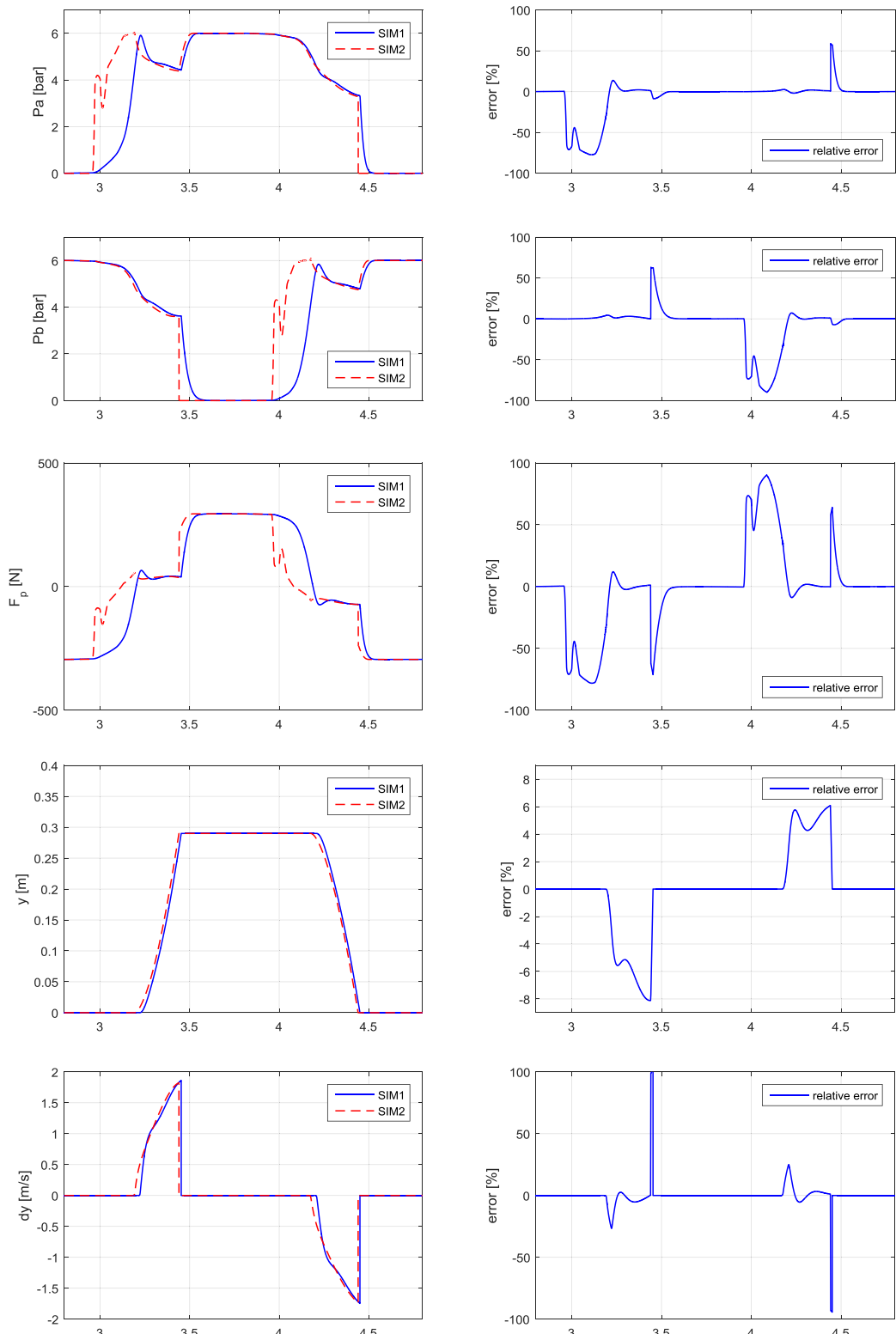
5. The influence of dead volume on system dynamics

There are three ISO standards regarding the cylinders with piston diameters from 8 to 320 mm and a maximum pressure of 10 bar. None of them contain specifications about dead volumes. According to the analysis conducted by Beater [13] on a set of 10 different cylinders with piston diameters of 32 mm and 40 mm the smallest dead volume is only 13% of the largest value. If the dynamic response of a cylinder has to be taken into account, this difference can become important.

Therefore, in this section the influence of dead volume on system dynamics will be investigated. In order to do that, the nonlinear model of the actuating system was implemented in MATLAB/Simulink based on the equations presented in Section 3 and ODE4 (Runge-Kutta) with a fixed-step size of 0.001 s was used as a solver for simulation purposes. The evaluation was performed in the following way. First the system model was simulated with a value of dead volumes close to zero and then with the values presented in Table 5. Relative error was used to compare the responses of chambers pressure, pneumatic force, position and velocity of the piston. Fig. 16 presents the final results. The following conclusions can be drawn. In the case of pressure and pneumatic force curves, the peak of relative error is the biggest as expected, around 80%, and this is because pressure dynamics and pneumatic force generated by the piston are directly influenced by the dead volumes. Piston velocity and position are influenced indirectly by dead volumes and therefore the peak of relative error is in the range of 20% for piston velocity and 6% for piston position. The 100% peaks on velocity graph near 3.5 s and 4.5 s are the result of phase difference between the two signals. Simulation results indicates that a proper identification of the dead volume can improve model accuracy in terms of pressure dynamics, piston velocity and piston position.

6. Model validation

Because mass flow parameters were identified using quasistatic pressure response inside a constant volume reservoir, an error analysis for measured vs. simulated pressure response was conducted. Flow mass parameters (A , b , a , m_s) were introduced in MATLAB/Simulink model using look-up tables and accuracy was tested using mean absolute error (MAE) and root mean squared error (RMSE). Fig. 17 presents the residuals analysis results plotted against input signal u . The MAE error is less than 0.04 bar in the range of 1–4.5 V and 5.5–10 V which means less than 1% if we consider that pressure supply was set to 7 bar (absolute). Spikes near 5 V (pneumatic center) are in dead zone range, a very nonlinear region. With a proper compensation scheme the influence of dead zone can be minimized and positioning accuracy improved. Experimental set-up from Fig. 7 was then used to investigate pressure response within the constant volume reservoir for a sinusoidal input signal u with a frequency of 4 Hz (Fig. 18).

**Fig. 16.** The influence of dead volume on system dynamics.

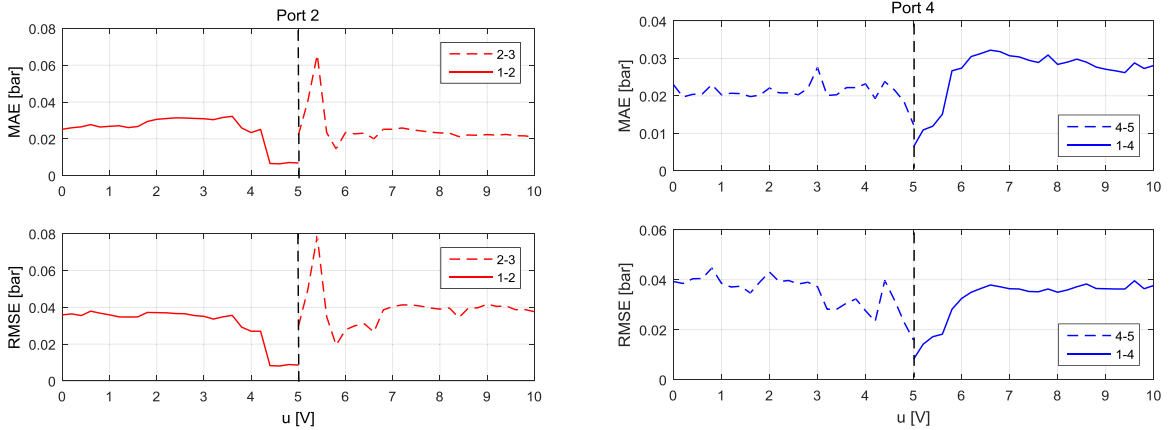


Fig. 17. Residuals analysis for mass flow characteristic.

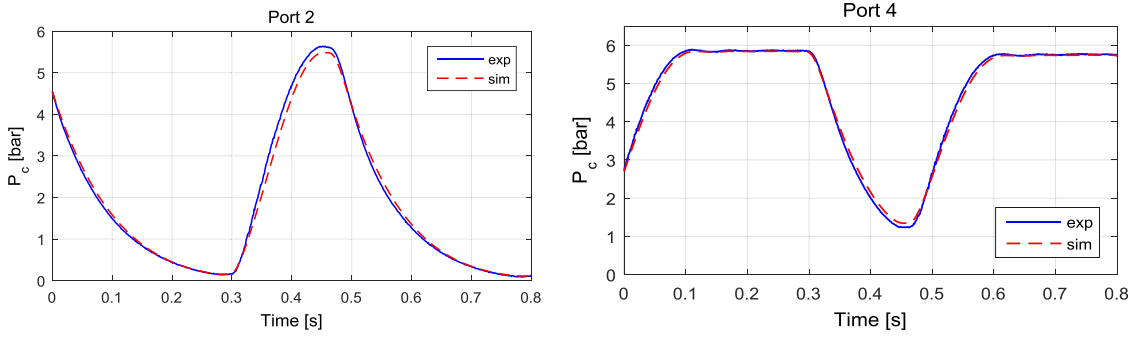


Fig. 18. Measured and simulated pressure response within the constant volume reservoir.

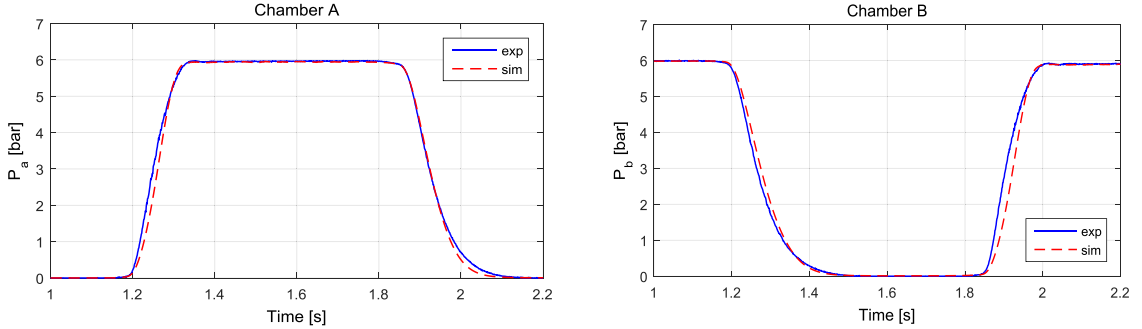


Fig. 19. Measured and simulated pressure response within actuator pneumatic chambers.

To validate flow model even further, experimental set-up from Fig. 1 was then used to compare pressure response for an input signal u with a frequency of 1 Hz when output ports of the valve were connected to actuator pneumatic chambers (Fig. 19). The obtained results demonstrates good agreement between simulation and experiment in both situations. The accuracy of the mass flow characteristic may be attributed to the improved model proposed in Section 3.

Next, the entire model was simulated using a sinusoidal input signal with a frequency of 0.5 Hz and position, velocity, chambers pressure and pneumatic force generated by the piston were plotted against experimental curves. Fig. 20 presents the results. The figures illustrates good agreement between the model and experiment. Table 7 presents the residual analysis results. The MAE for position is in the range of 0.2 mm, chambers pressure 0.1 bar and pneumatic force less than 9 N. Regarding comparative results, from authors knowledge only in two papers has been used for modelling purpose a pneumatic linear drive unit like the one presented in this work [3,15]. Plots presented by Meng et al. in [3] demonstrates good agreement between simulation and experimental results despite the fact that numerical values are not provided while Shu and Bone agreed in [15] that further improvements of their model are needed in order to obtain more accurate results with this type of actuators.

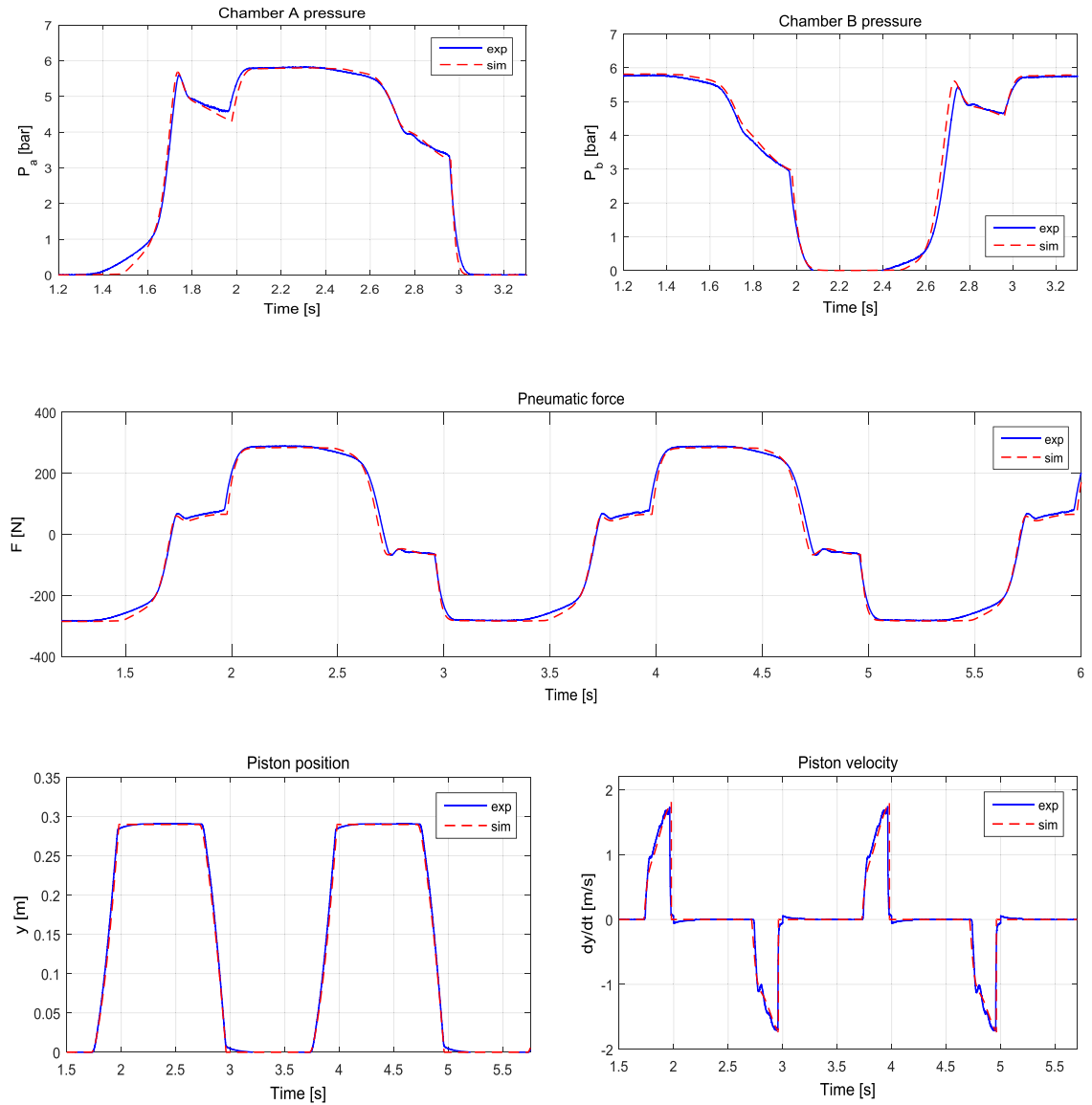


Fig. 20. Measured and simulated piston position and velocity, chambers pressure and pneumatic force.

Table 7
Residual analysis for simulates vs experimental position, velocity, chambers pressure and pneumatic force.

	MAE	RMSE
Piston position [mm]	0.25	0.46
Chamber A pressure [bar]	0.092	0.148
Chamber B pressure [bar]	0.115	0.209
Pneumatic force [N]	8.84	13.4

7. Conclusions

The key to design a high performance motion controller for servo-pneumatic systems is a good mathematical model and it seems that although many researches have been conducted in the last decade, positioning accuracy is far from perfect. Moreover linear actuators with high friction force and complex internal design implies bigger challenges in terms of modelling. In this context, the contribution of this paper has been to provide an improved nonlinear modelling and parameter

identification methodology of servo-pneumatic actuating systems that have into their structure linear pneumatic actuators with highly complex internal design and high friction force in order to be used for model-based design of high-accuracy motion control applications. Using standard orifice theory and ISO 6358-1:2013 mass flow characteristic has been accurately modeled in order to predict the combined effect of the multiple restrictions within the flow path, situation usually found in servo-pneumatic systems. Heat transfer and dead volumes were taken into account in thermodynamic model of the pneumatic chambers while piston friction force was modelled using elasto-plastic model, an improved version of LuGre friction force model that uses a continuous function proposed by to describe stiction more accurately. Dead volume influence on system dynamics was investigated and the conclusion is that a proper identification of the dead volume improves model accuracy in terms of pressure dynamics, piston velocity and piston position. In terms of performance, position error was less than 1%, chambers pressure error was 1.6% related to pressure supply and the pneumatic force error was 3% if we take into account the maximum theoretical force generated by piston. Based on the obtained results and the current level of precision for motion control applications from industry, the proposed methodology can be a good starting point to design better motion controllers in the field of servo-pneumatic positioning systems.

Acknowledgements

This paper was realized within the Partnerships Programme in priority domains-PN-II, which runs with the financial support of MEN-UEFISCDI, Project no. PN-II-PT-PCCA-2013-4-1629.

References

- [1] I.L. Krivts, G.V. Krejnin, Pneumatic actuating systems for automatic equipment, Structure and Design, Taylor & Francis Group LLC, 2006.
- [2] N. Alexandrescu, Mechatronic technology in the area of pneumatics – pneumronics, in: 6th Workshop on European Scientific and Industrial Collaboration on promoting Advanced Technologies in Manufacturing WESIC08, 2008, pp. 335–341.
- [3] D. Meng, G. Tao, J. Chen, W. Ban, Modeling of a pneumatic system for high-accuracy position control, in: International Conference on Fluid Power and Mechatronics (FPM), 2011, pp. 505–510.
- [4] A. Saleem, C.B. Wong, J. Pu, P.R. Moore, Mixed-reality environment for frictional parameters identification in servo-pneumatic system, *Simul. Pract. Theory* 17 (2009) 1575–1586, doi:[10.1016/j.simpat.2009.06.016](https://doi.org/10.1016/j.simpat.2009.06.016).
- [5] A. Saleem, B. Taha, T. Tutunjii, A. Al-Qaisia, Identification and cascade control of servo-pneumatic system using particle swarm optimization, *Simul. Pract. Theory* 52 (2015) 164–179, doi:[10.1016/j.simpat.2015.01.007](https://doi.org/10.1016/j.simpat.2015.01.007).
- [6] H.I. Ali, S.B.M. Noor, S.M. Bashi, M.H. Marhaban, A review of pneumatic actuators (modeling and control), *Aust. J. Basic Appl. Sci.* 3 (2009) 440–454.
- [7] M.F. Rahmat, S. Sunar, S.N. Salim, M.S.Z. Abidin, M. Fauzi, Z. Ismail, Review on modeling and controller design in pneumatic actuator control system, *Int. J. Smart Sens. Intell. Syst.* 4 (2011) 630–661.
- [8] Z. Rao, G.M. Bone, Nonlinear modeling and control of servo pneumatic actuators, *IEEE Trans. Control Syst. Technol.* 16 (2008) 562–569, doi:[10.1109/TCST.2007.912127](https://doi.org/10.1109/TCST.2007.912127).
- [9] P.G. Harris, G.E. O'Donnell, T. Whelan, Modelling and identification of industrial pneumatic drive system, *Int. J. Adv. Manuf. Technol.* 58 (2012) 1075–1086, doi:[10.1007/s00170-011-3447-7](https://doi.org/10.1007/s00170-011-3447-7).
- [10] J. Van der Merwe, C. Scheffer, Parameter identification and evaluation of a proportional directional flow control valve model, *R&D J. South Afr. Instit. Mech. Eng.* 29 (2013) 18–25. <http://hdl.handle.net/10019.1/94124>.
- [11] Pneumatic fluid power – Determination of flow-rate characteristics of components using compressible fluids – Part 1: General rules and test methods for steady-state flow. http://www.iso.org/iso/catalogue_detail.htm?csnumber=56612 (accessed 11.08.2016).
- [12] J.F. Carneiro, F.G. de Almeida, in: Reduced-order thermodynamic models for servopneumatic actuator chambers, 220, 2006, pp. 301–314, doi:[10.1243/09596518JCE203](https://doi.org/10.1243/09596518JCE203).
- [13] P. Beater, *Pneumatic drives: system design, Modelling and Control*, Springer Verlag, 2007.
- [14] A.J. Czmerk, Increasing of stiffness of double-acting pneumatic cylinder, *Analecta Technica Szegedinensis* 9 (2015) 39–45.
- [15] E. Richer, Y. Hurmuzlu, A high performance pneumatic force actuator system: part I– nonlinear mathematical model, *ASME J. Dyn. Syst. Measur. Control* 122 (2000) 416–425, doi:[10.1115/1.1286336](https://doi.org/10.1115/1.1286336).
- [16] N. Shu, G.M. Bone, Development of a nonlinear dynamic model for a servo pneumatic positioning system, in: Proc. Of the IEEE International Conference on Mechatronics&Automation, Niagara Falls, Canada, 2005, pp. 43–48, doi:[10.1109/ICMA.2005.1626520](https://doi.org/10.1109/ICMA.2005.1626520).
- [17] C.-R. Rad, O. Hancu, V. Maties, Experimental identification of dead volume in pneumatic linear drives, romanian review precision mechanics, *Opt. Mechatron.* 45 (2014) 49–53. ISSN: 2247-7063<https://www.scopus.com/inward/record.uri?eid=2-s2.0-84929430513&partnerID=40&md5=752b631f791e9e6962f887db35b79f24>.
- [18] B.M.Y. Nouri, F. Al-Bender, J. Swevers, P. Vanherck, H. Van Brussel, Modeling a pneumatic servo positioning system with friction, in: Proceedings of the American Control Conferenc, 2000, pp. 1067–1071, doi:[10.1109/ACC.2000.876664](https://doi.org/10.1109/ACC.2000.876664).
- [19] A.C. Valdiero, L.A. Rasia, Friction dynamics mathematical modeling in special pneumatic cylinder, in: 22nd International Congress of Mechanical Engineering (COBEM 2013), 2013, pp. 9155–9163.
- [20] J.W. Li1, X.B. Chen, Q. An, S.D. Tu, W.J. Zhang, Friction models incorporating thermal effects in highly precision actuators, *Rev. Sci. Instrum.* 80 (2009) 045104–1–045104–6 <http://dx.doi.org/10.1063/1.3115208>.
- [21] P. Dupont, B. Armstrong, V. Hayward, Elasto-plastic friction model: contact compliance and stiction, in: Proceedings of the American Control Conference, 2000, pp. 1072–1077.
- [22] P. Dupont, V. Hayward, B. Armstrong, F. Altpeter, Single state elastoplastic friction models, *IEEE Trans. Autom. Control* 47 (2002) 787–792, doi:[10.1109/TAC.2002.1000274](https://doi.org/10.1109/TAC.2002.1000274).
- [23] V. Hayward, B.S.R. Armstrong, F. Altpeter, P.E. Dupont, Discrete-time elasto-plastic friction estimation, *IEEE Trans. Control Syst. Technol.* 17 (2009) 688–696, doi:[10.1109/TCST.2008.2001710](https://doi.org/10.1109/TCST.2008.2001710).
- [24] R.R. Richter, A.C. Valdiero, Friction dynamics mathematical modeling in special pneumatic cylinder, *ABCM Symp. Series Mechatron.* 6 (2014) 800–808.
- [25] Linear drives DGPI/DGPIL, with integrated displacement encoder – FESTO catalogue https://www.festo.com/cat/en-gb_gb/data/doc_ENGB/PDF/EN_DGPIL_EN.PDF (accessed 11.08.2016).
- [26] Proportional directional control valves MPYE – FESTO catalogue https://www.festo.com/cat/en-gb_gb/data/doc_ENGB/PDF/EN_MPYE_EN.PDF (accessed 11.08.2016).
- [27] R. de Giorgi, N. Kobbi, S. Sesmat, E. Bideaux, Thermal model of a tank for simulation and mass flow rate characterization purposes, in: Proceedings of the 7th JFPS International Symposium on Fluid Power, 2008, pp. 225–230, doi:[10.5739/isfp.2008.225](https://doi.org/10.5739/isfp.2008.225).
- [28] R. de Giorgi, S. Sesmat, E. Bideaux, Using inverse models for determining orifices mass flow rate characteristics, in: Proceedings of the 6th JFPS International Symposium on Fluid Power, 2005, pp. 380–385, doi:[10.5739/isfp.2005.380](https://doi.org/10.5739/isfp.2005.380).

- [29] C.R. Rad, O. Hancu, C. Lapsan, Gray-box modeling and closed-loop temperature control of a thermotronic system, in: The 11th IFToMM International Symposium on Science of Mechanisms and Machines, Springer International Publishing, 2014, pp. 197–207, doi:[10.1007/978-3-319-01845-4_20](https://doi.org/10.1007/978-3-319-01845-4_20).
- [30] C.-R. Rad, O. Hancu, V. Maties, C. Lapsan, Parameter identification and modeling of a pneumatic proportional valve with applicability in control design of servo-pneumatic systems, Advanced Concepts in Mechanical Engineering – ACME 2014 658 (2014) 700–705, doi:[10.4028/www.scientific.net/AMM.658.700](https://doi.org/10.4028/www.scientific.net/AMM.658.700).
- [31] A.C. Valdiero, D. Bavaresco, P.I. Andriollo, Experimental identification of the dead zone in proportional directional pneumatic valves, Int. J. Fluid Power 9 (2008) 27–33, doi:[10.1080/14399776.2008.10781294](https://doi.org/10.1080/14399776.2008.10781294).
- [32] J.F. Carneiro, F.G. de Almeida, Heat transfer evaluation of industrial pneumatic cylinders, Proc. Instit. Mech. Eng. Part I 221 (2006) 119–128, doi:[10.1243/09596518JSCIE188](https://doi.org/10.1243/09596518JSCIE188).
- [33] A.C. Valdiero, C.S. Ritter, C.F. Rios, M. Rafikov, Nonlinear mathematical modeling in pneumatic servo position applications, Math. Probl. Eng. 2011 (2011) Article ID 472903, 16 pages, doi:[10.1155/2011/472903](https://doi.org/10.1155/2011/472903).